

# Nanoscale Advances

Volume 7  
Number 24  
21 December 2025  
Pages 7857–8172

[rsc.li/nanoscale-advances](https://rsc.li/nanoscale-advances)



ISSN 2516-0230

**PAPER**

Jeongwon Park, Michael Taeyoung Hwang *et al.*  
Plasmonic resonance modulation of graphene by nanoscale  
substrate curvatures

Cite this: *Nanoscale Adv.*, 2025, 7, 7899

# Plasmonic resonance modulation of graphene by nanoscale substrate curvatures

Vahid Faramarzi,<sup>a</sup> Sareh Vatani,<sup>b</sup> Mohsen Heidari,<sup>a</sup> Jeongwon Park <sup>\*b</sup> and Michael Taeyoung Hwang<sup>\*a</sup>

The nanopatterning of graphene with complex geometries and configurations has been widely investigated to excite plasmonic resonances in the graphene layer with high spatial confinement and gate tunability for nanophotonic applications. However, the existing approaches suffer from time-consuming and complicated fabrication processes, edge effects, and a narrow spectral tunability range of plasmonic resonances in graphene, limiting their utility in optoelectronic applications. Here, we study the effect of substrate corrugation and curvature on the plasmonic resonances of graphene through theoretical studies of a model system – graphene on closely packed SiO<sub>2</sub> nanospheres with different diameters. Highly confined plasmonic waves in graphene are efficiently excited due to nanoscale deformations in graphene using a nanocorrugated substrate on silicon. The SiO<sub>2</sub> nanospheres, with their close-packed curvature pattern, couple the incident optical wave to the graphene plasmonic resonances, thereby creating a sharp notch (resonance peak) on the normal-incidence transmission spectra (absorption spectra) with a high-quality factor of  $\sim 109$  and a near-field intensity enhancement of  $\sim 50^2$ . The resonant wavelength of the plasmonic modes can be tuned over a wide wavelength range in the mid-infrared by adjusting the size of the nanospheres. Finally, we demonstrate that the biaxially deformed graphene structure can detect slight variations in the refractive index of the surrounding analyte. The results demonstrate a high sensitivity of 3250 nm RIU<sup>-1</sup> and a large figure-of-merit of 63.2 RIU<sup>-1</sup> for deformed graphene on closely packed SiO<sub>2</sub> nanospheres. Our findings indicate that biaxially nanocorrugated graphene on closely packed SiO<sub>2</sub> nanospheres, with its facile fabrication process, strong plasmonic resonances, and superior sensing performance, provides a platform for ultrasensitive biosensing.

Received 12th May 2025  
Accepted 18th October 2025

DOI: 10.1039/d5na00470e

rsc.li/nanoscale-advances

## 1. Introduction

Surface plasmons (SPs), coupled electromagnetic excitation of photons and mobile charge carriers at the interface between a metal and a dielectric material, open exciting avenues to manipulate and control light confined in nanoscale devices.<sup>1</sup> However, plasmons in metals are not tunable and exhibit strong ohmic losses, which attenuate and limit the propagation lengths of SP waves.<sup>2</sup> The superior electronic properties of graphene, such as ultra-high mobility of charge carriers, low optical loss, high flexibility, and transparency, make it a promising plasmonic material to build integrated photonic devices for a broad spectral range from near-infrared to THz.<sup>3,4</sup> Due to its two-dimensional (2D) nature and high electrical conductivity, graphene supports plasmons with high spatial confinement and strong electric field enhancement.<sup>5–8</sup> Furthermore, the carrier density and chemical potential in graphene can be

tuned by electrical gating or chemical doping, offering the interesting opportunity to develop tunable plasmonic devices.<sup>3,9</sup> However, the future realization of graphene plasmonic platforms relies on converting incident light into propagating graphene plasmons (GPs). Due to a large mismatch between the GPs and incident light wave vectors, the coupling between SPs and free-space electromagnetic waves cannot be attained. Therefore, using a far-field method, the momentum of SPs and light can be matched, and a large wavelength of light turns into ultra-short GP wavelengths.<sup>10,11</sup> The plasmonic resonances in graphene can be excited in lithographically patterned structures using optical coupling configurations such as prism couplers, waveguide structures, and grating couplers.<sup>12–21</sup> However, the fabrication process of these optical couplers is time-consuming and not cost-effective; thus, realizing the broadband tunability of GPs over the infrared wavelength range is still challenging. Also, owing to their bulky (massive) configurations, they cannot be readily integrated with other electronic components and circuits. Rapid, cost-effective, and facile fabrication of photonic devices to excite plasmonic waves in graphene remains a challenge in developing graphene plasmonic circuits. Crumpled graphene structures have recently drawn significant attention

<sup>a</sup>Department of BioNano Technology, Gachon University, 1342 Seognam-Daero, Sujeong-Gu, Seongnam 13120, Republic of Korea. E-mail: anol81@gachon.ac.kr

<sup>b</sup>Department of Electrical and Biomedical Engineering, 1664 N. Virginia Street, Reno, NV 89557, USA. E-mail: jepark@unr.edu



as a new pathway to manipulate plasmonic resonances in graphene over a broad spectral wavelength range through mechanical reconfiguration of wrinkled structures.<sup>22</sup>

In our previous study, we also showed that biaxially crumpled graphene structures present a higher number of plasmonic modes with higher photo-absorption intensities and lower full-width at half-maximum (FWHM) values, indicating stronger plasmonic resonances as compared to the uniaxially crumpled graphene.<sup>23</sup> Although broadband tunability of plasmonic resonances can be achieved using crumpled graphene structures, GPs are largely affected by the high optical absorption of polymer-based substrates such as polydimethylsiloxane (PDMS) or a very high bond (VHB) layer in the mid-infrared region of light. In this frequency range, spectral overlap between the resonance wavelength of GPs and absorbance peaks of the substrate results in damping, attenuation, and broadening of the plasmonic resonances in the graphene layer.<sup>23</sup> Therefore, in such an interacting system, the plasmonic resonances of graphene are overwhelmed by the large optical response of the polymeric substrate, and distinct plasmon resonances in the graphene cannot be distinguished from the whole optical absorption of the system. Thus, these configurations present challenges in efficiently converting light into GPs, enhancing light-matter interactions, and realizing integrated graphene plasmonic devices with broadband tunability across the IR wavelengths. Recently, it has been shown that 3-dimensional wrinkled graphene can be created by deformations at the micro- and nanoscale on an undulating substrate made of closely packed SiO<sub>2</sub> nanospheres by inducing the strain and buckle delamination of the graphene layer.<sup>24</sup> The curving and bending of 2D materials and thin films can be engineered using this approach. The 3D deformation and adhesion of graphene on the SiO<sub>2</sub> nanospheres can be revealed by depositing graphene on the substrate. Therefore, regular biaxially wrinkled patterns are created in the graphene layer using graphene on the closely packed SiO<sub>2</sub> nanosphere structures. Thus, controllable deformed/wrinkled patterns in graphene can be engineered by transferring and depositing graphene on the substrate. The closely packed SiO<sub>2</sub> nanospheres on silicon (Si) perform as a biaxially corrugated substrate, such as a patterned optical configuration, to excite and launch the propagating GPs. Such deformed graphene as regularly curved or bent 2D layers has not yet been studied for designing plasmonic devices. Hence, we hypothesize that nanoscale deformation and bending of 2D graphene in 3-dimensions could result in distinct plasmonic resonances in graphene and modulation of their resonance wavelengths over a broad spectral range by controlling the size of SiO<sub>2</sub> nanospheres.

We propose using closely packed SiO<sub>2</sub> nanospheres on silicon as a symmetrical biaxially corrugated substrate to excite a guided-wave resonance in deformed and bent (wrinkled) graphene films. The guided mode resonance, which couples optical waves to the plasmonic waves, can be directly observed from the absorption spectra by creating a drastic variation in the optical/photo absorption intensity at the resonance wavelength. We show that strong plasmonic resonances with broadband tunability can be realized using controllable

deformed graphene structures on SiO<sub>2</sub> nanospheres with close-packed curvature patterns. The closely packed SiO<sub>2</sub> nanospheres, which perform as a tunable optical filter, can be readily tuned with a slight change in the energy Fermi level of the graphene layer. To investigate the modulation of plasmonic resonances in graphene, we systematically vary substrate corrugation features by changing the size/diameter of SiO<sub>2</sub> nanoparticles. Our proposed structure, consisting of graphene on spherical SiO<sub>2</sub> nanoparticles with minimum spacing and close-packing properties, is thus an ideal model system to study plasmonic resonances in graphene by converting optical waves into the propagating GPs, controlling their resonance frequency, and enhancing light-matter interactions. Owing to its facile fabrication process and reproducibility, the presented approach possesses several benefits over the conventional patterned graphene structures, such as nanoribbons. The method does not require electron beam lithography to pattern the nanoconfined graphene devices, and the realization of curved and wrinkled graphene is obtained by direct manipulation of the graphene layer. This results in nanoscale wrinkling features and deformation patterns in graphene, which create strong plasmonic resonances. Our results demonstrate that wrinkled/deformed graphene on SiO<sub>2</sub> nanospheres with close-packed curvature patterns is a new pathway for manipulating strong plasmonic resonances across a broad spectral range. The proposed structure can be utilized to build plasmonic-photonics circuits based on deformed 2D materials, such as ultrafast optical modulators, filters, and metamaterials. Finally, the potential application of this structure for biosensing is investigated by determining the shift in plasmonic resonance wavelength of the deformed graphene sensor in response to small variations in the refractive index of an analyte atop the graphene layer using theoretical calculations based on the semiclassical Drude model combined with the finite element method. We demonstrate that for a given change in the refractive index, the wavelength shift of the plasmonic resonance mode and the corresponding FOM are larger for deformed graphene compared to conventional graphene-based plasmonic devices. The proposed structure reveals its superiority regarding sensitivity, FOM, and quality factor (*Q*). Our findings indicate that the deformed graphene structure on SiO<sub>2</sub> nanospheres with a close-packed curvature pattern emerges as a promising platform for the development of ultrasensitive plasmonic biosensors with broadband tunability across the infrared light range.

## II. Physics

Doped graphene has garnered significant attention recently due to its exceptional electronic properties.<sup>25</sup> Theoretical studies have explored the propagation of highly confined plasmonic waves in graphene layers. This study employs full-wave 3D simulations using the finite element method within the COMSOL Multiphysics wave optics module to analyze plasmonic resonances in wrinkled graphene structures. The graphene layer is a thin film with two-dimensional surface conductivity aligned with the wrinkled configuration.



According to previous studies, the carrier mobility of flat graphene varies from 1000 cm<sup>2</sup> (V<sup>-1</sup> s<sup>-1</sup>) for chemical vapor deposition (CVD)-grown films to 230 000 cm<sup>2</sup> (V<sup>-1</sup> s<sup>-1</sup>) in suspended graphene obtained through exfoliation.<sup>26</sup> Based on this, we selected an intermediate mobility of 10 000 cm<sup>2</sup> (V<sup>-1</sup> s<sup>-1</sup>) for deformed graphene resting on closely packed SiO<sub>2</sub> nanospheres. The chemical potential of graphene was taken to be spatially uniform. This assumption is justified by a prior experimental study showing that back-gate tuning of curved graphene over nanospheres yields quasi-uniform Fermi level modulation.<sup>24</sup> Although local variations in the electric field may induce slight inhomogeneities in chemical potential, these are not expected to significantly impact the global plasmonic response in the regime considered.

Optical simulations were conducted with periodic boundary conditions imposed along the wrinkling direction to evaluate the far-field response of biaxially deformed graphene structures. SiO<sub>2</sub> nanospheres on a silicon substrate were chosen as the reference material to induce nanoscale deformations in the graphene layer, thereby enabling the excitation of surface plasmon resonances in the modified graphene channel.

In our simulations, graphene is defined using a transition boundary condition and modeled with an anisotropic dielectric function described by a diagonal permittivity tensor. The in-plane permittivity components are represented as

$$\varepsilon_{r11} = \varepsilon_{r22} = 2.5 + i \frac{\sigma_{\text{Gr}}}{\varepsilon_0 \omega t} \quad (1)$$

while the normal component to the surface is defined as  $\varepsilon_{r33} = 2.5$ ,  $\varepsilon_0$  is the vacuum permittivity and  $t$  represents the graphene thickness, which is considered to be 0.34 nm. As outlined in eqn (2), graphene's two-dimensional conductivity ( $\sigma_{\text{Gr}}$ ) is a complex quantity influenced by both intraband and interband processes, which vary depending on the incident photon energy. The intraband component eqn (3) reduces to the Drude model when the temperature approaches absolute zero ( $T = 0$  K), while the interband term eqn (4) corresponds to electron-hole pair generation and recombination.<sup>27–29</sup> In the mid-infrared region, the interband charge carrier transitions in graphene are ignored as the photon energy is less than  $2E_{\text{f}}$ . Thus, the intraband transitions can contribute to the surface conductivity of graphene.

$$\sigma_{\text{Gr}} = \sigma'_{\text{Gr}} + i\sigma''_{\text{Gr}} = \sigma_{\text{intra}} + \sigma_{\text{inter}} \quad (2)$$

$$\sigma_{\text{intra}} = \frac{ie^2 k_{\text{B}} T}{\pi \hbar^2 (\omega + i\tau^{-1})} \left[ \frac{E_{\text{f}}}{k_{\text{B}} T} + 2 \ln \left( \exp \left( \frac{-E_{\text{f}}}{k_{\text{B}} T} \right) + 1 \right) \right] \quad (3)$$

$$\sigma_{\text{inter}} = \frac{ie^2}{4\pi \hbar} \ln \left( \frac{2|E_{\text{f}}| - (\omega + i\tau^{-1})\hbar}{2|E_{\text{f}}| + (\omega + i\tau^{-1})\hbar} \right) \quad (4)$$

where  $k_{\text{B}}$  is the Boltzmann constant,  $T$  is the temperature,  $\hbar$  is the reduced Planck constant,  $\tau_{\text{g}}$  is the carrier relaxation time, which is related to the carrier mobility  $\mu_{\text{g}}$  in graphene as  $\tau_{\text{g}} = \mu_{\text{g}} E_{\text{f}} / e v_{\text{f}}^2$ , and  $E_{\text{f}} = \hbar v_{\text{f}} \sqrt{\pi n_{\text{g}}}$  is the Fermi energy level in graphene,  $v_{\text{f}} = 10^6$  m s<sup>-1</sup> is the Fermi velocity,  $n_{\text{g}}$  is the carrier density in graphene. For graphene with high doping levels or subjected to an external electric field, the condition  $E_{\text{f}} \gg k_{\text{B}} T$

holds, and the term  $\ln \left( \exp \left( \frac{-E_{\text{f}}}{k_{\text{B}} T} \right) + 1 \right) \approx 0$ . In the simulations, graphene is modeled using the standard complex surface conductivity without explicit inclusion of strain-dependent permittivity. This assumption is valid within the low strain regime (<2%), as reported experimentally,<sup>24</sup> where the deformation primarily affects curvature-induced field localization rather than significantly altering the electronic band structure or optical response, demonstrating that such strain corrections yield nearly identical plasmonic spectra. Therefore, the effect of strain on the absorption spectrum is negligible, and the dominant factor controlling the plasmon resonance is the geometrical modulation of graphene curvature, which perturbs the effective local dielectric environment and enables phase-matching to incident radiation.

Corrugated structures are employed to address the mismatch between the wave vector of free-space electromagnetic waves and plasmons. These structures are achieved by transferring graphene onto an array of nanospheres with the close-packed curvature patterns, which induce strain in graphene. Upon releasing the strain, deformations and wrinkles naturally form in the graphene film. Under normal incidence, plasmonic energy dissipation in 2D materials causes a distinct resonance peak in the absorption spectrum near the resonant frequency. The target sensing medium is positioned on top of the wrinkled structure for bio-sensing applications. In undulated configurations, the wrinkles are filled with the substrate material. The refractive index of the sensing medium is selected to correspond with commonly studied biomolecules such as human serum albumin, single-stranded DNA, and double-stranded DNA.

A periodic port is implemented in the  $z$ -direction to illuminate the structure, with periodic boundary conditions applied along the wrinkling directions ( $x$  and  $y$  axes) to simulate an infinitely periodic array of unit cells. A transverse electric field propagates along the wrinkles, radiating perpendicularly to the structure. To optimize computational efficiency, a non-uniform mesh is employed. The graphene boundaries along the  $x$  and  $y$  axes are refined to a resolution of 0.1 nm, while mesh sizes gradually increase outside the graphene region with a growth factor of 1.5. The maximum mesh element size was 100 nm, and a mid-infrared light irradiates the structure from the top port. The simulation runs until the system achieves convergence.

The scattering ( $S$ ) parameters of the device were determined using the finite element method. These parameters are utilized to extract the effective refractive index of plasmonic sensors and to characterize the optical properties, including transmission, reflection, and absorption spectra. The transmission and reflection coefficients are computed as

$$T_{\text{f}} = |S_{21}|^2, R_{\text{f}} = |S_{11}|^2$$

and the corresponding absorption is determined by

$$A_{\text{f}} = 1 - T_{\text{f}} - R_{\text{f}}$$

The overall absorption spectrum is derived by solving Maxwell's equations while enforcing boundary conditions for



graphene conductance and permittivity, and the refractive indices of silicon and SiO<sub>2</sub> substrates in mid-infrared were taken from Kischkat.<sup>30</sup> Graphene on the closely packed SiO<sub>2</sub> nanospheres can be fabricated using widely reported techniques that are both cost-effective and scalable. Close-packed SiO<sub>2</sub> nanosphere monolayers can be prepared on silicon substrates using the spin-coating technique. The method allows the formation of periodic curvature patterns with nanometer control over sphere diameter. Monolayer graphene, typically grown by chemical vapor deposition (CVD), can be transferred onto the nanosphere layer using a polymer-supported wet transfer method (*e.g.*, PMMA-assisted transfer). Upon contact, the graphene drapes over the nanospheres due to van der Waals attraction and capillary forces during the drying process. To improve adhesion and eliminate polymer residues, an annealing step in forming gas or vacuum can be used to enhance graphene conformality over the nanoscale curvature.

### III. Results and discussion

We investigated the plasmonic resonances of wrinkled graphene structures on closely packed SiO<sub>2</sub> nanospheres on a silicon substrate. To excite surface plasmons in graphene, the wavevector of the corrugated structure in the form of closely packed nanospheres can compensate for the wavevector mismatches. Our plasmonic device comprises a wrinkled graphene layer placed on periodic spherical SiO<sub>2</sub> nanoparticles with close-packed curvature patterns on the mid-infrared transparent silicon substrate (Fig. 1). Wrinkled graphene is assumed to adopt a biaxial sinusoidal shape with geometrical parameters, including wrinkle period ( $T_g$ ) and wrinkle height ( $H_g$ ) equal to the radius of the nanospheres ( $R_s$ ). The distance between the centers of two adjacent spheres is defined as the period of the structure, *i.e.*  $T_g = 2 \times R_s = D_s$ , where  $D_s$  is the diameter of the nanospheres.

The electronic properties of graphene are defined in Table 1. Transverse magnetic (TM) polarized light along the wrinkling

directions  $x$  and  $y$  illuminates the system in the normal direction to the structure ( $K_0$ ). First, we performed full-wave optical simulations to investigate the far-field spectral response of biaxially wrinkled graphene. To observe the plasmonic resonances in the proposed wrinkled graphene structures, we have studied the absorption and transmission spectra of the device at normal incidence with the E-field polarization along the wrinkling directions,  $x$ -axis and  $y$ -axis, as shown in Fig. 1.

The simulated normal-incidence absorption spectra of a free-standing biaxially wrinkled graphene structure for the incident electric field ( $E_{\text{inc}}$ ) parallel ( $E_{\text{inc}} \parallel \lambda_w$ ) and perpendicular ( $E_{\text{inc}} \perp \lambda_w$ ) to the wrinkling direction ( $\lambda_w$ ) are shown in Fig. 2(a). Multiple resonance peaks, including the first- and second-order plasmonic modes, are observed in the optical absorption spectrum for  $E_{\text{inc}} \parallel \lambda_w$ , whereas no plasmonic resonance peak is observed for  $E_{\text{inc}} \perp \lambda_w$ . First, one can see two absorbance peaks at the resonance wavelengths of  $\sim 7$  and  $\sim 4.8$   $\mu\text{m}$ , corresponding to the first and second plasmonic modes of the free-standing biaxially wrinkled graphene flake with a structural period of 150 nm in Fig. 2(a), respectively. The resonance peaks in the absorption spectrum are attributed to resonant plasmonic modes confined in the deformed graphene structures.

To model the performance of a physically realizable plasmonic device, we simulated the deformed graphene structures on SiO<sub>2</sub> nanospheres (Gr-SiO<sub>2</sub>NS<sub>s</sub>) with close-packed curvature patterns. The wrinkled structure on closely packed nanospheres couples free space optical waves to graphene plasmons propagating in-plane, thereby creating a strong change in the optical absorption spectrum at the resonant wavelength. One can see sharp resonance peaks from biaxially deformed graphene on closely packed SiO<sub>2</sub> nanospheres for  $E_{\text{inc}} \parallel \lambda_w$ . Two sharp resonances in the absorption spectrum around 7.25 and 4.9  $\mu\text{m}$  corresponding to the first and second plasmonic modes in graphene can be observed in Fig. 2(b) for the wrinkled graphene on a periodic spherical curvature pattern of SiO<sub>2</sub> nanospheres. The spectral window with a central wavelength of around 9  $\mu\text{m}$  and a spectral width of 2  $\mu\text{m}$  in Fig. 2(b) is attributed to the phonon mode of SiO<sub>2</sub> nanospheres. Also, the normal-incidence transmission spectrum of the deformed Gr-SiO<sub>2</sub>NS<sub>s</sub> structure is shown in Fig. 2(c). The peak of the maximum optical absorption (the main resonance notch in the transmission spectrum) shows the most efficient coupling of the incident light to the graphene plasmon. The  $Q$ -factor was determined from the simulated transmission spectra using the standard definition:

$$Q = \frac{\lambda_{\text{res}}}{\text{FWHM}}$$

Table 1 The electronic parameters of graphene

Definition	Label	Value	Unit
Carrier density	$n_g$	$3.01 \times 10^{13}$	$\text{cm}^{-2}$
Fermi velocity	$v_f$	$10^6$	$\text{m s}^{-1}$
Fermi energy level	$E_f$	0.64	eV
Carrier mobility	$\mu_g$	10 000	$\text{cm}^2 (\text{V}^{-1} \text{s}^{-1})$
Carrier relaxation time	$\tau_g$	0.64	Ps
Temperature	$T$	300	K

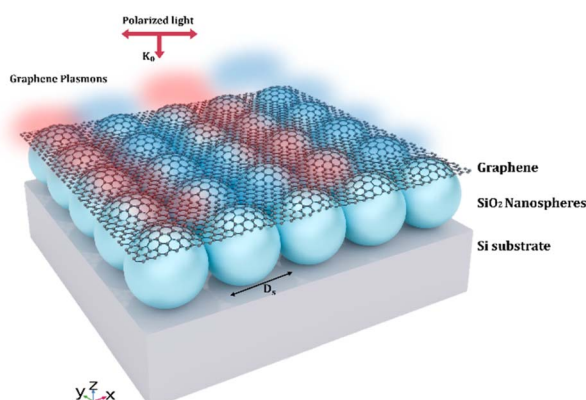


Fig. 1 Schematic demonstration of a deformed graphene structure on closely packed SiO<sub>2</sub> nanospheres with wrinkle period  $D_s$  on a silicon substrate. Polarized light with the electric field along the wrinkling directions  $x$  and  $y$  irradiates in the normal direction  $K_0$  to the structure to excite graphene plasmons.



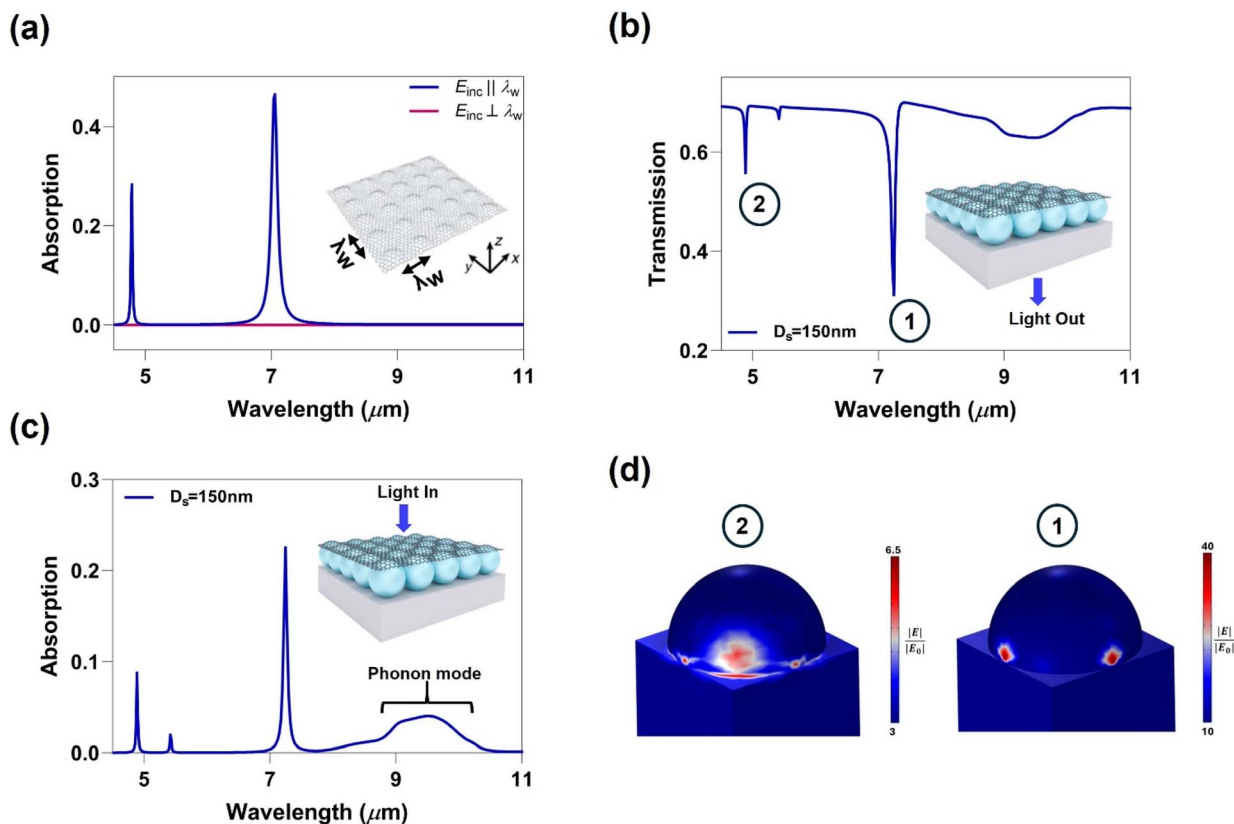


Fig. 2 Optical absorption spectra of (a) a free-standing biaxially deformed graphene structure with  $\lambda_w = 150$  nm, where  $\lambda_w$  is the corrugated wavelength, for  $E_{inc} \parallel \lambda_w$  (blue) and  $E_{inc} \perp \lambda_w$  (red). The inset shows a schematic illustration of the biaxially deformed graphene structure. Absorption (b) and transmission (c) spectra of a biaxially deformed graphene structure on close-packed  $\text{SiO}_2$  nanosphere arrays with  $D_s = 150$  nm. The insets show the schematic illustration for the biaxially deformed graphene structure on closely packed  $\text{SiO}_2$  nanospheres. (d) Near-field intensity distributions of the first and second graphene plasmon modes at resonance wavelengths of 7.25 and 4.9  $\mu\text{m}$ , respectively.

where  $\lambda_{res}$  is the central resonance wavelength of the plasmon mode and FWHM is the full width at half maximum of the same dip. The sharp notches in the transmission spectrum of closely packed Gr- $\text{SiO}_2\text{NS}_s$  possess an extinction ratio of  $\sim 4$  dB and a quality factor ( $Q$ ) of  $\sim 109$ , which is larger than that of graphene and metal mid-infrared plasmonic structures.<sup>31–37</sup> This relatively low-loss optical configuration allows us to build an ultracompact resonator or filter with high- $Q$ . A minor spectral feature appears near 5.4  $\mu\text{m}$  between the two dominant plasmonic resonances. This peak is attributed to either a weak hybridized mode formed by coupling between adjacent curvature-induced plasmonic states, or to partial destructive interference effects resulting in an asymmetric Fano-type profile. This mode is not a primary plasmonic resonance but arises from the complex electromagnetic environment shaped by nanoscale curvature. The near-field intensity distribution profiles of the fundamental and second-order modes at wavelengths of 7.25 and 4.9  $\mu\text{m}$  in one period are shown in Fig. 2(d).

To assess the role of graphene curvature on plasmonic performance and near-field enhancement, we carried out control simulations for three representative configurations: (I) flat graphene on  $\text{SiO}_2$  disks, (II) flat graphene on  $\text{SiO}_2$  nanospheres, and (III) corrugated graphene conformally draped over  $\text{SiO}_2$  nanospheres. All structures were modeled with identical

sphere or disk diameters, lattice periodicity, and simulation parameters to ensure a direct comparison.

The results clearly indicate that flat graphene, whether supported on disks or spheres, exhibits only very weak resonances around 4.5  $\mu\text{m}$  for  $D_s = 120$  nm with broadband absorption features predominantly governed by the intrinsic phonon resonances of  $\text{SiO}_2$  in the 8–10  $\mu\text{m}$  range, and negligible spectral tunability upon changing the nanostructure size, as shown in Fig. 3. In stark contrast, the corrugated graphene configuration produces a sharp, high-intensity plasmonic peak whose resonance wavelength redshifts systematically with increasing sphere diameter. The corresponding near-field profiles reveal highly localized plasmonic “hot spots” along the curved graphene surface at the ridge region (Fig. 3(d)). However, for planar graphene cases, fields are weakly localized and distributed diffusely over the surface, with no pronounced hotspot formation (Fig. 3(b) and (c)).

Quantitatively, both the peak absorption intensity and the localized electric field enhancement for corrugated graphene are nearly an order of magnitude larger than those for flat graphene under otherwise identical conditions. This demonstrates that biaxial deformation and curvature not only facilitate efficient excitation of graphene plasmon modes but also significantly boost vertical field confinement and light-plasmon





**Fig. 3** (a) Comparative optical response and near-field distributions for three substrate configurations: flat graphene on SiO<sub>2</sub> disks (red curves), flat graphene on SiO<sub>2</sub> nanospheres (blue curves), and corrugated graphene on SiO<sub>2</sub> nanospheres (black curves) for sphere diameters  $D_s = 60$ ,  $90$ , and  $120$  nm. The left panels present the simulated absorption spectra, highlighting the emergence of distinct plasmonic modes (I–III) for each configuration and the SiO<sub>2</sub> phonon band. The right panels show the corresponding normalized electric-field intensity distributions  $|E|/|E_0|$  for each mode at  $D_s = 120$  nm for (b) flat graphene on SiO<sub>2</sub> disks, (c) flat graphene on SiO<sub>2</sub> nanospheres, and (d) corrugated graphene on SiO<sub>2</sub> nanospheres. The corrugated graphene reveals substantially stronger and spectrally sharper plasmonic resonances compared to flat-graphene configurations, with near-field enhancement and photoabsorption intensity approaching an order of magnitude higher.

coupling strength. The resulting strong resonances in the absorption spectra, combined with the enhanced near-field localization, are central to the large spectral tunability and subsequently the sensing capabilities observed in the corrugated system—performance metrics that cannot be achieved in planar graphene geometries.

The curvature radii of the nanospheres used in this study (10–200 nm), combined with the measured adhesion mechanics of graphene, ensure that the induced tensile strain remains modest, typically  $<1\text{--}2\%$ , even at the sphere apexes. In this regime, the relative change in Fermi velocity is below 2%, which would produce a plasmon frequency shift of only a few percent, well within the numerical uncertainty of our full-wave simulations and smaller than the intrinsic linewidth of the resonances investigated. Previous experimental and theoretical studies have shown that such moderate, non-uniform strains do not substantially alter the optical conductivity or Drude weight of monolayer graphene.<sup>24</sup> Similarly, it has also been demonstrated that including strain-corrected conductivity in crumpled graphene models produces negligible differences compared to strain-free calculations. For this reason, and to isolate the influence of curvature-induced phase matching, we have

neglected explicit strain-dependent conductivity in our modeling. The absorption spectra and plasmonic resonances in our system are therefore governed primarily by geometric modulation of the graphene surface, which alters the effective dielectric environment and enables momentum matching to incident radiation.

Unlike uniaxial (1D) corrugations, which provide in-plane momentum only along a single direction and thus restrict coupling to one set of diffraction orders, biaxial periodicity supplies reciprocal lattice vectors along both principal axes and their diagonals. This expanded momentum space enables coupling to a higher set of plasmon modes, including diagonal and hybrid orders that are symmetry-forbidden in uniaxial geometries. The result is a denser and higher modal spectrum, as well as additional features, such as the intermediate resonance, which can be observed near  $5.4\ \mu\text{m}$  (Fig. 2(c)).

Biaxial curvature also promotes mode coupling between orthogonal plasmonic flow channels, producing hybridized resonances, mode splitting near avoided crossings, particularly in the vicinity of the SiO<sub>2</sub> phonon band, and enhanced far-field coupling due to the larger number of Fourier components matching the incident field. Near-field distributions in biaxial



geometries further differ from their uniaxial counterparts; instead of concentrating fields solely along ridges or valleys, the biaxial surface forms saddle points and two-dimensional cavity-like regions that confine energy in both directions. This increases the active graphene area participating under resonant conditions, enhances optical absorption at major resonances, improves the near-field enhancement, and, in certain symmetry-protected configurations, narrows linewidths *via* quasi-bound-state-in-continuum effects. These enhancements arise entirely from the geometry-driven momentum matching and mode hybridization enabled by the biaxial symmetry, not from intrinsic material changes, reaffirming the validity of our modeling assumptions.<sup>23</sup>

With this confirmation, we focus on the strongest plasmonic resonance in subsequent investigations. We explore how the plasmonic resonances are influenced by the size of SiO<sub>2</sub> nanospheres and their close-packed curvature patterns. Here, the period of the structure is equal to the diameter of SiO<sub>2</sub> nanospheres ( $T_g = D_s$ ). We observe the optical absorption for different diameters ( $D_s$ ) of SiO<sub>2</sub> nanospheres. As seen in Fig. 4(a), the resonance wavelength of plasmonic modes redshifted from  $\sim 2$  to  $\sim 7.25$   $\mu\text{m}$  with increasing  $D_s$  from 10 to 150 nm. The scaling of the resonant wavelength with respect to the nanospheres period,  $T_g = D_s$ , is shown in Fig. 4(b). The optical absorption intensity also increased with larger  $D_s$  from 10 to 150 nm.

Moreover, near-field distributions of the fundamental mode for graphene plasmons varied with the size of SiO<sub>2</sub> nanospheres (Fig. 4(c)). An enhanced near-field intensity near the valley regions between nanospheres was exhibited with decreasing  $D_s$ . Owing to higher confinement of graphene plasmons in the immediate vicinity of smaller spheres, the near-field is locally

enhanced at the nanoscale compared to larger spheres; such plasmons are strongly confined and sensitive to the size. A maximum near-field intensity enhancement of  $\sim 100^2$  in the valley regions of deformed graphene structures with  $D_s = 10$  nm. Our results demonstrated the tunability of plasmonic resonances observed in far-field absorption spectra and corresponding near-field field enhancement profiles by nanoscale deformation modulation of graphene controlled by nanosphere curvatures.

Another parameter that affects the plasmonic resonances is the distance between the graphene-covered SiO<sub>2</sub> nanospheres in the form of a graphene gap ( $G_g$ ) or an air gap ( $G_a$ ). To demonstrate this, we first assume a small graphene gap (continuous graphene) between SiO<sub>2</sub> nanospheres, while the size of the spheres is fixed, which creates an array of nanospheres covered by a graphene film with a structural period of  $T_g = D_s + G_g$ , as shown in Fig. 5(a).

Introducing such a gap reduces the overlap between the graphene plasmonic wave and the SiO<sub>2</sub> nanospheres, and therefore, the effective strength of the nanospheres. Fig. 5(b) shows the absorption intensity drops when the gap between the nanospheres is increased ( $D_s = 150$  nm), but the optical intensity remains high when  $G_g$  is less than 7.5 nm. The resonance wavelength blue shifts from  $\sim 7.25$  to  $\sim 6.61$   $\mu\text{m}$  as  $G_g$  increases to 25 nm, because the effective refractive index of plasmon modes (the structure) becomes smaller. Since the distance between the nanospheres is typically just a few nanometres, the spectral shape and the absorption intensity of the plasmonic resonances are very close to those with close-packed curvature patterns (without the gap). In comparison, the periodic dielectric SiO<sub>2</sub> nanospheres with the close-packed curvature structure excite plasmonic waves in a continuous graphene

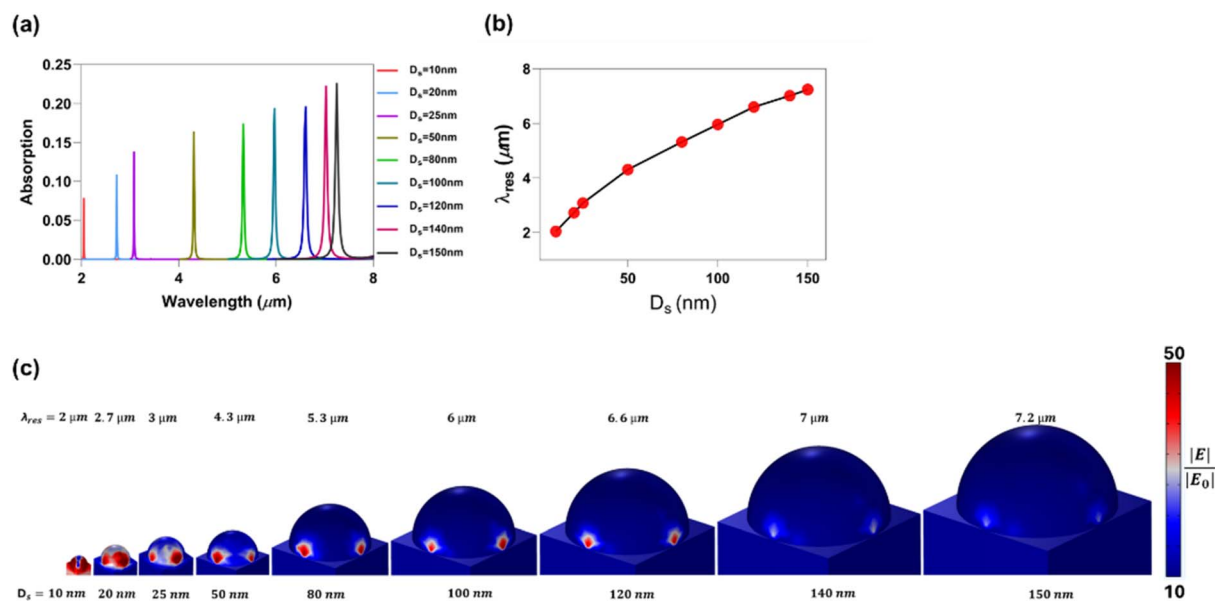


Fig. 4 (a) Optical absorption spectra for the biaxially corrugated graphene structure on closely packed SiO<sub>2</sub> nanospheres with varying  $D_s$  from 10 to 150 nm. (b) Scaling of the fundamental-mode resonant wavelength with respect to  $D_s$ . (c) Near-field distributions normalized by the incident field ( $E_0$ ) in the biaxially corrugated graphene structures at the resonance wavelength of the fundamental plasmonic mode  $\lambda_{\text{res}}$  for different  $D_s$  ranging from 10 to 150 nm.



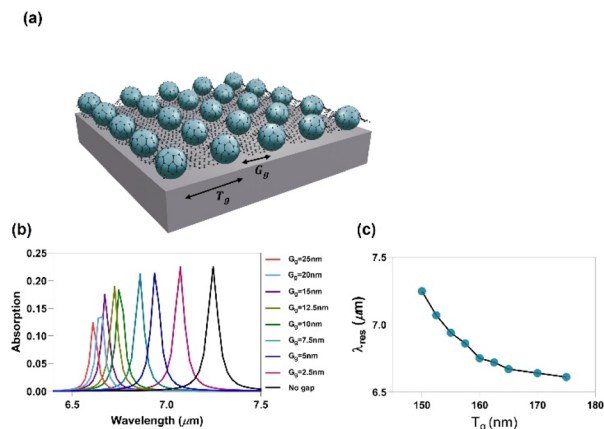


Fig. 5 (a) Schematic demonstration of a biaxially deformed graphene structure on the SiO<sub>2</sub> nanospheres with a graphene gap  $G_g$  and wrinkle period  $T_g = D_s + G_g$ . (b) Optical absorption spectra for the wrinkled graphene structure with varying  $G_g$  from 0 to 25 nm at  $D_s = 150$  nm. (c) Scaling of the fundamental-mode resonant wavelength with respect to wrinkle period  $T_g$ .

film, and the resonant wavelength is determined by the size of the spheres. When there is no gap between the spheres, the resonant wavelength red shifts as the period increases. However, when the size of the nanospheres is fixed, the resonant wavelength blueshifts as the gap between the spheres and thus the period increases. The scaling of the resonant wavelength with respect to the structural period for closely packed Gr-SiO<sub>2</sub>NS<sub>s</sub> (Fig. 4(b)) is opposite to the scaling rule of Gr-SiO<sub>2</sub>NS<sub>s</sub> with a graphene gap (Gr-SiO<sub>2</sub>NS<sub>s</sub>- $G_g$ ), as shown in Fig. 5(c). The difference between the curves in Fig. 4(b) and 5(c) arises from the effective strength of plasmon excitation by nanospheres and also changes in the effective index of the plasmonic mode, which increases with the occupation ratio of the high-index material SiO<sub>2</sub>.

Next, we add a small air gap ( $G_a$ ), in the form of a discontinuity in graphene, between SiO<sub>2</sub> nanospheres while graphene remains on top of the nanospheres (Gr-SiO<sub>2</sub>NS<sub>s</sub>- $G_a$ ), and no graphene exists between them (hemisphere graphene shell). This will create a periodic structure of isolated nanoconfined Gr-SiO<sub>2</sub>NS<sub>s</sub> with a period of  $T_g = D_s + G_a$  to realize its bound electron oscillations (Fig. 6(a)). Here, the radius of the nanospheres is fixed, while the gap between the nanospheres, and thus the period of the array, is changed. One can see two distinct plasmonic resonances in Fig. 6(b), which are created as a result of the mode splitting phenomenon by the optical phonon mode of SiO<sub>2</sub> spheres at  $\sim 9$   $\mu\text{m}$ .

Two singular peaks at the edges of Gr-SiO<sub>2</sub>NS<sub>s</sub> with a  $D_s$  of 80 nm, around the wavelengths of 7.9 and 10.85  $\mu\text{m}$ , can be observed in Fig. 6(b) for a  $G_a$  of 5 nm. The observed photo-absorption spectra are due to the excitation of the bound electron oscillations in the isolated graphene hemisphere nanoshells, which is governed by the density of free electrons in the graphene and have similar features to those of the closely packed Gr-SiO<sub>2</sub>NS<sub>s</sub> structure demonstrated in Fig. 2. Due to the finite dimensions of graphene when patterned to nanoscale

structures such as nanoribbons or nanoparticles, the movement of the free charge carriers is restricted in the graphene plane. This results in the formation of bound electrons, which support resonant oscillation modes (edge plasmon modes) and can be excited by normal-incidence photons. These bound electron oscillations, which occur at the edge of a patterned graphene nanostructure, create edge plasmon resonances. A sharp resonance mode with ER  $\sim 4.2$  dB and  $Q \sim 53$  can be observed in the transmission spectrum in Fig. 6(c). The near-field intensity distributions of the edge plasmon modes at wavelengths of 7.9 and 10.85  $\mu\text{m}$  are shown in Fig. 6(d).

Due to scattering electron-phonon interactions in the Gr-SiO<sub>2</sub>NS<sub>s</sub> structure, the bound electron resonant mode is split, with the SiO<sub>2</sub> phonon mode between them ( $\sim 9$   $\mu\text{m}$ ). When the nanospheres are placed close to each other, the radiation from neighbouring spheres can destructively interfere for the odd mode at the far field in the normal direction. Thus, only even modes can be excited by the vertically incident radiation. Therefore, due to the interference effects, only the even mode contributes to the resonant notch (peak) observed in the transmission (absorption) spectra. Fig. 6(e) shows how the coupling between the nanospheres affects the resonance of the sphere array, where the radius of the spheres remains constant while the gap between them (period of the array) is varied. Fig. 6(e) illustrates that the resonant wavelength exponentially blue-shifts as the gap between nanospheres increases. This shift occurs due to the decreasing coupling strength between the nanospheres as the gap increases. Therefore, the optical coupling between the plasmonic resonance modes at the graphene edges exponentially enhances as the gap shrinks. As seen in Fig. 6(e), for the edge plasmon mode at 10.85  $\mu\text{m}$ , the absorption intensity increases to  $\sim 0.2$  and its resonant wavelength red-shifts from 10.33 to 10.86  $\mu\text{m}$  by shrinking  $G_a$  from 150 to 5 nm. For the first plasmon mode at 7.9  $\mu\text{m}$ , a spectral change behaviour similar to Gr-SiO<sub>2</sub>NS<sub>s</sub> with a graphene gap (previous structure) was observed. Fig. 6(f) shows that the scaling rule of the resonant wavelength of the edge plasmon mode as the period increases, which follows an exponential dependency. For a large gap, the resonant wavelength approximates that of a single Gr-SiO<sub>2</sub>NS (plasmon mode at the edge of the graphene nanostructure), which is marked as the dashed red line in Fig. 6(f). Our results show that deformation induced by SiO<sub>2</sub> nanospheres with close-packed curvature patterns of different sizes enables broad spectral tunability for plasmonic resonances from mid- to near-infrared.

As can be seen in Fig. 4(b) and 6(f), the scaling rule for closely packed graphene-covered nanospheres is opposite to that of isolated nanoconfined graphene-covered nanospheres with an air gap separation, revealing the fundamental difference between these two structures. In the former structure, the periodic nanospheres with the close-packed curvature patterns act as a wavevector matching component to excite the plasmonic waves in the graphene layer, in which the size of the nanospheres is the determining factor for the resonant frequency. The resonances of the isolated nanoconfined graphene-covered nanospheres with air-gap separation are due to



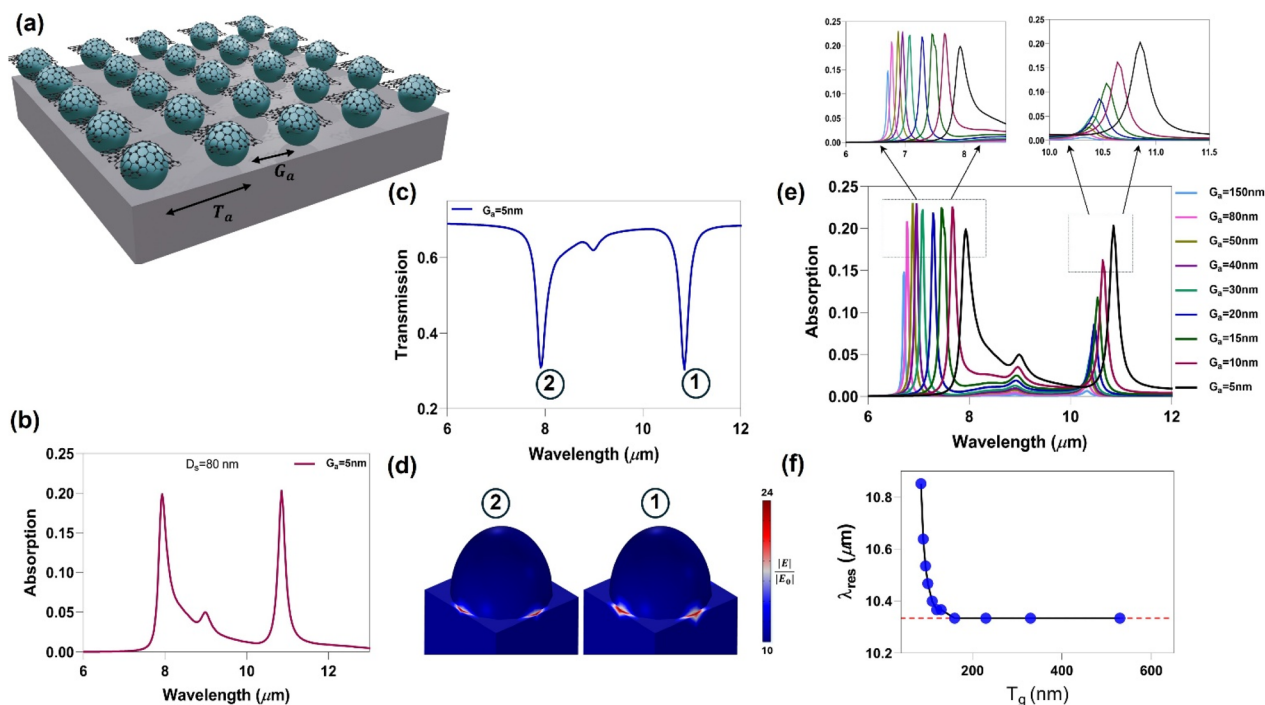


**Fig. 6** (a) Schematic demonstration of biaxially deformed graphene structures on the SiO<sub>2</sub> nanospheres with an air gap  $G_a$  and wrinkle period  $T_g = D_s + G_a$ . Optical absorption (b) and transmission (c) spectra for the corrugated graphene structures with  $D_s = 80$  nm and  $G_a = 5$  nm. (d) Near-field intensity distributions of the edge graphene plasmon modes at resonance wavelengths of 7.9 and 10.85  $\mu\text{m}$ , respectively. (e) Optical absorption spectra for the corrugated graphene structures with varying  $G_a$  from 5 to 150 nm and  $D_s = 80$  nm. The upper plots show a zoomed-in view of the resonance wavelength shifts of the edge plasmon modes by varying  $G_a$ . (f) Scaling of the resonance wavelength of the edge plasmon mode at 10.85  $\mu\text{m}$  with respect to wrinkle period  $T_g$ .

the bound electron oscillation, which is tuned mainly by the width of the gap.

By adjusting the Fermi level in graphene, the electrical tuning of plasmonic resonances of the deformed graphene structure on the closely packed SiO<sub>2</sub> nanospheres can be achieved. Through a small change in the Fermi level, the wide tuning range for the plasmon resonances is obtained, as shown in Fig. 7. When the Fermi level of graphene changes from 0.54 eV to 0.74 eV, it induces the resonance wavelength to shift by 863 nm, from  $\sim 7$   $\mu\text{m}$  to  $\sim 6.137$   $\mu\text{m}$  for a  $D_s$  of 120 nm, which is comparable to that achieved for graphene on the silicon diffractive grating and higher than that in crumpled graphene

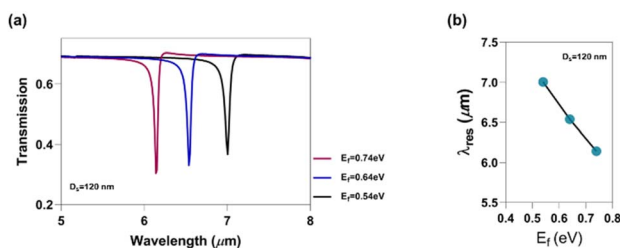


**Fig. 7** (a) Normal-incidence transmission spectra of biaxially corrugated graphene structures on the close-packed SiO<sub>2</sub> nanospheres with different Fermi energy levels  $E_f$  in graphene when  $D_s = 120$  nm. (b) Scaling of the fundamental-mode resonant wavelength with respect to  $E_f$ .

structures on the polymeric substrates, enabling it to build highly tunable optical filters and modulators.<sup>38</sup>

Next, we explore the potential application of a deformed graphene structure on the SiO<sub>2</sub> nanospheres with a close-packed curvature pattern as a plasmonic biosensor. We proceed to investigate how the plasmonic resonances are influenced by analyte solutions introduced into the deformed graphene structure by calculating the wavelength shifts in the plasmonic resonance modes upon changes in the refractive index of the solution. For a given nanosphere size, the plasmon resonances of deformed graphene can strongly overlap with the wide spectral peak corresponding to phonon modes of SiO<sub>2</sub> nanospheres in the mid-infrared range, which results in damping, broadening, and attenuation of the plasmon modes. This negatively affects the performance of the plasmonic device, especially for biosensing applications where the high-quality plasmon resonance modes with high optical absorption intensities and narrower frequency widths (lower FWHM values) are required, as these modes facilitate monitoring of spectral shifts of plasmonic resonances induced by slight variations in the refractive index of the surrounding medium. The high-Q factor and strong plasmonic resonances of our proposed structure make it a promising platform to develop highly sensitive plasmonic biosensors for a wide wavelength range in mid-infrared, where it is particularly desired for biosensing, as the vibrational fingerprints of biomolecule building blocks, such as proteins and DNA, lie in this frequency range. Upon the variation in



biomolecule concentration, a local change is induced in the effective refractive index at the analyte-graphene interface, thereby affecting the propagation constant of plasmonic waves and eventually resulting in spectral shifts in the resonance wavelength of surface plasmons. The sensing parameters, including figure of merit (FOM) and sensitivity ( $S_T$ ), are calculated to evaluate the performance of the proposed structures. The sensitivity is defined as the resonance wavelength shift over the change in refractive index,  $S_T = \delta\lambda_{\text{res}}/\delta n$ , and figure of merit,  $\text{FOM} = S_T (\text{nm RIU}^{-1})/\text{FWHM} (\text{nm})$ ,<sup>39</sup> as the ratio of the sensor sensitivity to the full width at half maximum (FWHM) of the resonant spectral peak, which quantifies the broadening of the resonant mode and therefore the resolution of the sensor for detection of refractive index variations.

The transmission spectra of the proposed structures under normal incidence have been investigated to obtain plasmonic resonances in biaxially deformed graphene in the presence of an analyte solution, as the refractive index of the solution ( $n_m$ ) above the graphene is changed. Fig. 8 compares the transmission spectra of deformed graphene structures on the SiO<sub>2</sub> nanospheres with the close-packed pattern, 5 nm-graphene gap, and 5 nm-air gap as the RI of the medium atop the surface of the graphene varies ( $n_m$ ) from 1.3 to 1.5. The shift in resonance wavelength of the main plasmon resonance for deformed graphene on SiO<sub>2</sub> nanospheres with a close-packed pattern ( $D_s = 50$  nm), a graphene gap of 5 nm, and an air gap of 5 nm was 650, 550, and 470 nm, respectively, which corresponds to the sensor

sensitivity of 3250 (FOM of 63.2), 2750 (69), and 2350 nm RIU<sup>-1</sup> (15.3 RIU<sup>-1</sup>), respectively. The higher sensitivity of Gr-SiO<sub>2</sub>NS<sub>s</sub> with a close-packed curvature pattern is attributed to the substantial overlap between the plasmonic wave and the adjacent Gr-SiO<sub>2</sub>NS<sub>s</sub>, thereby creating highly confined plasmonic resonance modes between nanospheres with strong local field enhancement, narrow spectral peaks, and high absorption intensity.

Compared to the close-packed Gr-SiO<sub>2</sub>NS<sub>s</sub> sensor, the sensitivity of Gr-SiO<sub>2</sub>NS<sub>s</sub> with an air gap (Gr-SiO<sub>2</sub>NS<sub>s</sub>-G<sub>a</sub>) is lower as edge plasmon modes (bound electron oscillations) are locally confined at the edge of isolated Gr-SiO<sub>2</sub>NS<sub>s</sub>, and therefore, less sensitive to the surrounding medium. Fig. 8 compares near-field enhancement of Gr-SiO<sub>2</sub>NS<sub>s</sub> structures with three different patterns. One can indeed see a higher local field enhancement of  $\sim 53^2$  for the closely packed Gr-SiO<sub>2</sub>NS<sub>s</sub> structure, as compared to the other two structures with a gap between nanospheres. The higher field enhancement of Gr-SiO<sub>2</sub>NS<sub>s</sub> with a close-packed curvature pattern confirms the results of superior sensing performance of this structure.

The close-packed nanosphere configuration represents the most straightforward and cost-effective platform among the three geometries studied. Monolayers of monodisperse silica nanospheres can be assembled on Si/SiO<sub>2</sub> substrates *via* established methods such as Langmuir-Blodgett (LB) deposition or spin coating, followed by direct transfer of CVD-grown monolayer graphene. These methods have been extensively



Fig. 8 Normal-incidence optical transmission spectra of biaxially corrugated graphene structures on SiO<sub>2</sub> nanosphere arrays with  $D_s = 60$  nm and (a) a close-packed curvature pattern, (b) a graphene gap  $G_g$ , and (c) an air gap  $G_a$  of 5 nm when the refractive index of the sample medium atop the graphene surface  $n_m$  changes from 1.3 to 1.5. The panels on the right compare the near-field intensity distributions at the plasmonic resonance wavelengths of the fundamental plasmon mode for the biaxially corrugated graphene structures denoted in (a)–(c) when  $n_m = 1.3$ . (d) Scaling of the fundamental-mode resonant wavelength with respect to  $n_m$  for structures denoted in (a)–(c).



**Table 2** Comparison of the sensing performance of the proposed wrinkled graphene structure with recently published refractive index sensors in the mid-infrared region

Recently published refractive index sensors	Resonant wavelength ( $\mu\text{m}$ )	Max sensitivity ( $\text{nm RIU}^{-1}$ )	Max FOM ( $\text{RIU}^{-1}$ )
Multimode interference in tellurite no-core optical fibers (2023) <sup>40</sup>	4–5	3069.1	22
Implanted cavities in metal-insulator-metal (MIM) waveguide (2019) <sup>41</sup>	2.75	2602.5	13
Resonant toroidal plasmonic metasensor (2019) <sup>42</sup>	5.5	2500	4
Metal-insulator-metal waveguide-based square-ring resonator plasmonic refractive index sensor (2024) <sup>43</sup>	3.6	2700	8.1
Fano-resonance plasmonic nanosensor based on a tapered waveguide cavity resonator (2024) <sup>44</sup>	2.52	2544.3	40.54
Silicon-on-insulator ring resonator plasmonic sensor based on graphene and gold nano-discs (2024) <sup>45</sup>	1.645	730	56.15
Hybrid plasmonic sensor based on graphene and an array of asymmetric gold nano-antennas (2019) <sup>46</sup>	7.2	2300	28.75
Graphene-decorated grating on a high dielectric substrate (2019) <sup>47</sup>	5.5	2780	17
Graphene-based diffractive grating structure (2017) <sup>48</sup>	9.5	2000	14.2
Dual-band graphene metamaterials (2019) <sup>49</sup>	7.85	2880	12.9
<b>Wrinkled graphene structures on SiO<sub>2</sub> nanospheres with a close-packed curvature pattern (this study)</b>	5.5	3250	63.2

demonstrated in previous studies and are compatible with wafer-scale integration using roll-to-roll or assisted assembly techniques.<sup>24</sup> The process requires no lithography, involves low-cost consumables, and is well within the capabilities of standard nano/microfabrication facilities, enabling high yield, scalability, and reproducibility.

The graphene-gap configuration, consisting of a non-close-packed nanosphere array with controlled interparticle spacing, can be fabricated using well-established approaches that preserve long-range hexagonal order while introducing uniform gaps between spheres. A common route involves first assembling a close-packed nanosphere monolayer *via* LB or optimized spin coating, followed by isotropic sphere shrinkage through controlled wet etching (*e.g.*, BOE/HF for silica spheres) to open the gaps without disturbing the lattice pitch. Alternatively, template-guided assembly can be employed, wherein lithographically defined pits or adhesion sites with slightly larger pitch than the sphere diameter enable deterministic placement of each nanosphere at a fixed separation. In all cases, the resulting lattice can be mechanically stabilized by a thin conformal dielectric coating (*e.g.*, 5–10 nm Al<sub>2</sub>O<sub>3</sub> by ALD) prior to graphene transfer. CVD graphene is then transferred using the standard PMMA-assisted method, conformally draping over the nanospheres and spanning the engineered gaps.

The air-gap configuration is experimentally feasible but presents the highest fabrication complexity. One route involves template-guided nanosphere assembly with e-beam lithographically defined pitch, followed by CVD graphene transfer and reactive ion etching (RIE), using oxygen plasma and the nanospheres as an etch mask to remove interstitial graphene. The graphene remaining atop the nanospheres is thereby removed over the etched regions, creating well-defined air gaps.

The graphene-gap geometry provides precise control over vertical separation between graphene and nanospheres, enabling systematic modulation of plasmon–substrate coupling strength, investigation of strong-to-weak coupling transitions,

and benchmarking of near-field confinement effects under controlled dielectric environments. The decoupling effect in this structure, while slightly lowering near-field intensity at the analyte interface, reduces substrate phonon–plasmon interactions, narrows resonance linewidths, and enhances spectral selectivity—beneficial for distinguishing biomolecules with closely spaced vibrational signatures.

The air-gap configuration, in which graphene conformally follows nanosphere curvature and leaves voids between spheres, modifies the effective dielectric environment and generates localized hotspots at graphene edges and in intersphere gaps. These regions enable a new functional sensing modality and yield edge-selective enhancement advantageous for detecting analytes that bind preferentially at defects, edges, or confined spaces. Furthermore, the reduced graphene–substrate contact in this geometry mitigates adsorption-induced doping and charge trapping, thereby improving chemical stability, minimizing contamination, and enhancing operational repeatability in fluidic sensing environments. Consequently, these alternative configurations expand the functional design space for mid-IR graphene plasmonics, enabling targeted trade-offs between sensitivity, selectivity, spectral resolution, and long-term stability. In summary, the latter two substantially expand the accessible parameter space for graphene plasmonics, introduce tunable vertical coupling, enable coupled plasmon–phonon mode control, and provide unique environmental sensing capabilities. Nevertheless, an important outcome of this study is the demonstration that the close-packed nanosphere configuration, despite its facile fabrication process, delivers superior biosensing performance, underscoring its practical relevance for scalable, high-performance graphene-based plasmonic devices.

Compared with graphene-based biosensors in the infrared light reported in the literature, our proposed structure presents superior sensing performance, in terms of sensor sensitivity and FOM. Table 2 compares the sensing performance of the



proposed deformed graphene biosensor with recently published graphene-based refractive index sensors.

The 3-dimensional (3D) configuration of the biaxially deformed graphene in our structure provides (allows) more cross-sectional surface area of graphene in contact with analytes (biomolecules) in all directions, especially near grooves and ridges of the deformed nanostructure. In contrast, strong potential confinement and local near-field enhancements occur. This results in enhanced sensing performance of plasmonic devices based on deformed graphene structures. With its superior metrics, facile fabrication, and broadband spectral tunability, we expect our proposed structure to help design new plasmonic biosensors based on deformed graphene channels.

## IV. Conclusions

We proposed a plasmonic device based on a biaxially corrugated graphene structure on the closely packed SiO<sub>2</sub> nanospheres. The nanoscale deformation of graphene created (formed) by nanospheres with a close-packed curvature pattern is responsible for creating (generating) strong plasmonic resonances. The biaxially deformed graphene structures, with varying wrinkle periods and heights by the size of nanospheres, enabled the manipulation of plasmonic resonances over a broadband tunable wavelength range. The substrate corrugation and spherical curvature of periodic nanospheres coupled far-field incident light to the graphene plasmonic waves, efficiently exciting resonance modes with strong confinement in deformed graphene structures. The strong plasmonic resonances enabled sharp notches in optical transmission with a quality factor of ~109 and optical absorption enhancements of up to ~0.3, as well as high near-field enhancements of ~50<sup>2</sup> for biaxially deformed graphene flakes. Furthermore, we showed strong light-matter interactions for the deformed graphene flakes on the nanocorrugated SiO<sub>2</sub> substrate, which enabled high sensitivity of the plasmonic device to ambient refractive index by inducing a large shift in the resonant wavelength. High sensitivity on the order of 3250 nm RIU<sup>-1</sup> has been obtained for the main resonance peaks of deformed graphene structures on corrugated SiO<sub>2</sub> nanospheres with a close-packed curvature pattern corresponding to a FOM of 63.2 RIU<sup>-1</sup>. With its strong plasmonic resonances and high sensitivity, our wrinkled graphene structures can be considered a promising platform for developing simple, high-performance, and ultrasensitive chemical and biological sensors based on plasmonic waves.

## Conflicts of interest

There are no conflicts to declare.

## Data availability

The data that support the findings of this study are available from the corresponding author upon reasonable request.

## Acknowledgements

This work was partly supported by the National Science Foundation (NSF Convergence Accelerator L476) under Grant ITE-2344476, NSF Award #2243754, and the Bean Space Foundation. J. Park acknowledges support from the Global Research Program through the National Research Foundation of Korea (RS-2025-02303505).

## References

- 1 H. Raether, *Plasmons on smooth and rough surfaces and on gratings*, Springer tracts in modern physics, 1988.
- 2 S. A. Maier, *Plasmonics: fundamentals and applications*, Springer, 2007, vol. 1.
- 3 R. R. Nair, P. Blake, A. N. Grigorenko, K. S. Novoselov, T. J. Booth, T. Stauber, N. M. R. Peres and A. K. Geim, Fine structure constant defines visual transparency of graphene, *Science*, 2008, **320**, 1308.
- 4 F. Bonaccorso, Z. Sun, T. Hasan and A. C. Ferrari, Graphene photonics and optoelectronics, *Nat. Photonics*, 2010, **4**, 611–622.
- 5 A. N. Grigorenko, M. Polini and K. S. Novoselov, Graphene plasmonics, *Nat. Photonics*, 2012, **6**, 749–758.
- 6 G. W. Hanson, Dyadic Green's functions and guided surface waves for a surface conductivity model of graphene, *J. Appl. Phys.*, 2008, **103**, 064302.
- 7 M. Jablan, H. Buljan and M. Soljačić, Plasmonics in graphene at infrared frequencies, *Phys. Rev. B: Condens. Matter Mater. Phys.*, 2009, **80**, 245435.
- 8 V. Faramarzi, V. Ahmadi, M. Heidari, B. Fotouhi and M. T. Hwang, Interband plasmon-enhanced optical absorption of DNA nucleobases through the graphene nanopore, *Opt. Lett.*, 2021, **47**, 194–197.
- 9 F. H. L. Koppens, D. E. Chang and F. J. García de Abajo, Graphene plasmonics: a platform for strong light-matter interactions, *Nano Lett.*, 2011, **11**, 3370–3377.
- 10 Z. Fei, A. S. Rodin, G. O. Andreev, W. Bao, A. S. McLeod, M. Wagner, L. M. Zhang, Z. Zhao, M. Thiemens and G. Dominguez, Gate-tuning of graphene plasmons revealed by infrared nano-imaging, *Nature*, 2012, **487**, 82–85.
- 11 P. Alonso-González, A. Y. Nikitin, F. Golmar, A. Centeno, A. Pesquera, S. Vélez, J. Chen, G. Navickaite, F. Koppens and A. Zurutuza, Controlling graphene plasmons with resonant metal antennas and spatial conductivity patterns, *Science*, 2014, **344**, 1369–1373.
- 12 J. Zhang, L. Zhang and W. Xu, Surface plasmon polaritons: physics and applications, *J. Phys. D Appl. Phys.*, 2012, **45**, 113001.
- 13 H. Yan, T. Low, W. Zhu, Y. Wu, M. Freitag, X. Li, F. Guinea, P. Avouris and F. Xia, Damping pathways of mid-infrared plasmons in graphene nanostructures, *Nat. Photonics*, 2013, **7**, 394–399.
- 14 L. Ju, B. Geng, J. Horng, C. Girit, M. Martin, Z. Hao, H. A. Bechtel, X. Liang, A. Zettl and Y. R. Shen, Graphene plasmonics for tunable terahertz metamaterials, *Nat. Nanotechnol.*, 2011, **6**, 630–634.



- 15 S. Thongrattanasiri, A. Manjavacas and F. J. García de Abajo, Quantum finite-size effects in graphene plasmons, *ACS Nano*, 2012, **6**, 1766–1775.
- 16 K. Y. M. Yeung, J. Chee, H. Yoon, Y. Song, J. Kong and D. Ham, Far-infrared graphene plasmonic crystals for plasmonic band engineering, *Nano Lett.*, 2014, **14**, 2479–2484.
- 17 Z. Fang, S. Thongrattanasiri, A. Schlather, Z. Liu, L. Ma, Y. Wang, P. M. Ajayan, P. Nordlander, N. J. Halas and F. J. García de Abajo, Gated tunability and hybridization of localized plasmons in nanostructured graphene, *ACS Nano*, 2013, **7**, 2388–2395.
- 18 P. A. D. Gonçalves, E. J. C. Dias, S. Xiao, M. I. Vasilevskiy, N. A. Mortensen and N. M. R. Peres, Graphene plasmons in triangular wedges and grooves, *ACS Photonics*, 2016, **3**, 2176–2183.
- 19 H. Yan, X. Li, B. Chandra, G. Tulevski, Y. Wu, M. Freitag, W. Zhu, P. Avouris and F. Xia, Tunable infrared plasmonic devices using graphene/insulator stacks, *Nat. Nanotechnol.*, 2012, **7**, 330–334.
- 20 P. Liu, W. Cai, L. Wang, X. Zhang and J. Xu, Tunable terahertz optical antennas based on graphene ring structures, *Appl. Phys. Lett.*, 2012, **100**, 153111.
- 21 V. Faramarzi, M. Heidari and M. T. Hwang, Plasmonic biosensor based on metal antenna on graphene for detection and counting of nanoparticles, *Hybrid Advances*, 2023, **3**, 100046.
- 22 V. Faramarzi, V. Ahmadi, M. T. Hwang and P. Snapp, Highly sensitive crumpled 2D material-based plasmonic biosensors, *Biomed. Opt. Express*, 2021, **12**, 4544–4559.
- 23 V. Faramarzi, M. Heidari, N. H. b. N. Zulkarnine and M. T. Hwang, Plasmonic biosensors based on deformed graphene, *Biophysica*, 2022, **2**, 538–547.
- 24 Y. Zhang, M. Heiranian, B. Janicek, Z. Budrikis, S. Zapperi, P. Y. Huang, H. T. Johnson, N. R. Aluru, J. W. Lyding and N. Mason, Strain modulation of graphene by nanoscale substrate curvatures: a molecular view, *Nano Lett.*, 2018, **18**, 2098–2104.
- 25 J. Yao, H. Wang, M. Chen and M. Yang, Recent advances in graphene-based nanomaterials: properties, toxicity and applications in chemistry, biology and medicine, *Microchim. Acta*, 2019, **186**, 1–25.
- 26 K. I. Bolotin, K. J. Sikes, Z. Jiang, M. Klima, G. Fudenberg, J. Hone, P. Kim and H. L. Stormer, Ultrahigh electron mobility in suspended graphene, *Solid State Commun.*, 2008, **146**, 351–355.
- 27 G. W. Hanson, Quasi-transverse electromagnetic modes supported by a graphene parallel-plate waveguide, *J. Appl. Phys.*, 2008, **104**, 084314.
- 28 K. Qin, B. Xiao and R. Sun, Mode analysis and research on graphene nanoribbons parallel-plate waveguide, *Micro Nano Lett.*, 2015, **10**, 558–560.
- 29 H. Lu, X. Gan, D. Mao and J. Zhao, Graphene-supported manipulation of surface plasmon polaritons in metallic nanowaveguides, *Photonics Res.*, 2017, **5**, 162–167.
- 30 J. Kischkat, S. Peters, B. Gruska, M. Semtsiv, M. Chashnikova, M. Klinkmüller, O. Fedosenko, S. Machulik, A. Aleksandrova and G. Monastyrskiy, Mid-infrared optical properties of thin films of aluminum oxide, titanium dioxide, silicon dioxide, aluminum nitride, and silicon nitride, *Appl. Opt.*, 2012, **51**, 6789–6798.
- 31 R. Yu, J. D. Cox, J. R. M. Saavedra and F. J. García de Abajo, Analytical modeling of graphene plasmons, *ACS Photonics*, 2017, **4**, 3106–3114.
- 32 S. Kim, M. S. Jang, V. W. Brar, Y. Tolstova, K. W. Mauser and H. A. Atwater, Electronically tunable extraordinary optical transmission in graphene plasmonic ribbons coupled to subwavelength metallic slit arrays, *Nat. Commun.*, 2016, **7**, 12323.
- 33 S. Kim, M. S. Jang, V. W. Brar, K. W. Mauser, L. Kim and H. A. Atwater, Electronically tunable perfect absorption in graphene, *Nano Lett.*, 2018, **18**, 971–979.
- 34 Z. Fei, M. D. Goldflam, J.-S. Wu, S. Dai, M. Wagner, A. S. McLeod, M. K. Liu, K. W. Post, S. Zhu and G. Janssen, Edge and surface plasmons in graphene nanoribbons, *Nano Lett.*, 2015, **15**, 8271–8276.
- 35 N. Verellen, P. Van Dorpe, C. Huang, K. Lodewijks, G. A. E. Vandenbosch, L. Lagae and V. V. Moshchalkov, Plasmon line shaping using nanocrosses for high sensitivity localized surface plasmon resonance sensing, *Nano Lett.*, 2011, **11**, 391–397.
- 36 V. A. Fedotov, M. Rose, S. L. Prosvirnin, N. Papasimakis and N. I. Zheludev, Sharp trapped-mode resonances in planar metamaterials with a broken structural symmetry, *Phys. Rev. Lett.*, 2007, **99**, 147401.
- 37 C. Wu, A. B. Khanikaev, R. Adato, N. Arju, A. A. Yanik, H. Altug and G. Shvets, Fano-resonant asymmetric metamaterials for ultrasensitive spectroscopy and identification of molecular monolayers, *Nat. Mater.*, 2012, **11**, 69–75.
- 38 W. Gao, J. Shu, C. Qiu and Q. Xu, Excitation of plasmonic waves in graphene by guided-mode resonances, *ACS Nano*, 2012, **6**, 7806–7813.
- 39 J.-T. Lin, D.-C. Cheng, M. Jiang, Y.-S. Chiang and H.-W. Liu, Analysis of Scaling Law and Figure of Merit of Fiber-Based Biosensor, *J. Nanomater.*, 2012, **2012**, 154736.
- 40 D. Song, W. Liu, Z. Yin, Q. Wang, X. Yan, X. Zhang, F. Wang, T. Suzuki, Y. Ohishi and T. Cheng, Mid-infrared refractive index sensor with high sensitivity and wide detection range based on multimode interference in tellurite optical fibers, *Results in Optics*, 2023, **12**, 100458.
- 41 A. Hocini, M. N. Temmar and D. Khedrouche, Design of mid infrared high sensitive metal-insulator-metal plasmonic sensor, *Chin. J. Phys.*, 2019, **61**, 86–97.
- 42 A. Ahmadivand, B. Gerislioglu, Z. Ramezani and S. A. Ghoreishi, Attomolar detection of low-molecular weight antibiotics using midinfrared-resonant toroidal plasmonic metachip technology, *Phys. Rev. Appl.*, 2019, **12**, 034018.
- 43 S. Guchhait, S. Chatterjee, T. Chakravarty and N. Ghosh, A metal-insulator-metal waveguide-based plasmonic refractive index sensor for the detection of nanoplastics in water, *Sci. Rep.*, 2024, **14**, 21495.



- 44 G. K. Yadav and S. K. Metya, Fano-resonance-based plasmonic refractive index sensor with high sensitivity for detection of urea, *J. Opt. Soc. Am. B*, 2024, **41**, 175–182.
- 45 T. Intisar, A. S. Alam, I. Hoque and M. O. Faruque, Numerical analysis of a highly sensitive SOI MRR refractive index sensor with performance enhancement using graphene and gold, *Heliyon*, 2024, **10**, e26186.
- 46 Q. Hong, J. Luo, C. Wen, J. Zhang, Z. Zhu, S. Qin and X. Yuan, Hybrid metal-graphene plasmonic sensor for multi-spectral sensing in both near-and mid-infrared ranges, *Opt. Express*, 2019, **27**, 35914–35924.
- 47 K. Tong, Y. Wang, F. Wang, J. Sun and X. Wu, Surface plasmon resonance biosensor based on graphene and grating excitation, *Appl. Opt.*, 2019, **58**, 1824–1829.
- 48 V. Faramarzi, V. Ahmadi, F. Ghane Golmohamadi and B. Fotouhi, A biosensor based on plasmonic wave excitation with diffractive grating structure, *Sci. Iran.*, 2017, **24**, 3441–3447.
- 49 S. Gong, B. Xiao, L. Xiao, S. Tong, S. Xiao and X. Wang, Hybridization-induced dual-band tunable graphene metamaterials for sensing, *Opt. Mater. Express*, 2019, **9**, 35–43.

